









Monoallelic *de novo* variants in *DDX17* cause a neurodevelopmental disorder

Eleanor G. Seaby,^{1,2,†} Annie Godwin,^{3,†} Géraldine Meyer-Dilhet,^{4,†} Valentine Clerc,^{5,†} Xavier Grand,^{5,6} Tia Fletcher,³ Laloe Monteiro,⁴ Martijn Kerkhofs,⁴ Valerio Carelli,^{7,8} Flavia Palombo,⁷ Marco Seri,⁹ Giulia Olivucci,⁹ Mina Grippa,⁹ Claudia Ciaccio,¹⁰ Stefano D'Arrigo,¹⁰  Maria Iascone,¹¹ Marion Bermudez,¹² Jan Fischer,¹² Nataliya Di Donato,¹² Sophie Goesswein,¹² Marco L. Leung,¹³ Daniel C. Koboldt,¹⁴ Cortlandt Myers,¹⁵ Gudny Anna Arnadottir,¹⁶  Kari Stefansson,¹⁶  Patrick Sulem,¹⁶  Ethan M. Goldberg,^{17,18} Ange-Line Bruel,^{19,20} Frederic Tran-Mau-Them,^{19,20} Marjolaine Willems,²¹ Hans Tomas Bjornsson,²² Hakon Bjorn Hognason,²² Eirny Tholl Thorolfsson,²²  Emanuele Agolini,²³ Antonio Novelli,²³ Giuseppe Zampino,^{24,25} Roberta Onesimo,²⁶ Katherine Lachlan,^{1,27} Diana Baralle,¹ Heidi L. Rehm,^{2,28} Anne O'Donnell-Luria,^{2,28,29} Julien Courchet,⁴ Matt Guille,³  Cyril F. Bourgeois^{5,‡} and Sarah Ennis^{1,‡}

†,‡These authors contributed equally to this work.

DDX17 is an RNA helicase shown to be involved in critical processes during the early phases of neuronal differentiation. Globally, we compiled a case series of 11 patients with neurodevelopmental phenotypes harbouring *de novo* monoallelic variants in *DDX17*. All 11 patients in our case series had a neurodevelopmental phenotype, whereby intellectual disability, delayed speech and language, and motor delay predominated.

We performed *in utero* cortical electroporation in the brain of developing mice, assessing axon complexity and outgrowth of electroporated neurons, comparing wild-type and *Ddx17* knockdown. We then undertook *ex vivo* cortical electroporation on neuronal progenitors to quantitatively assess axonal development at a single cell resolution. Mosaic *ddx17* crispants and heterozygous knockouts in *Xenopus tropicalis* were generated for assessment of morphology, behavioural assays and neuronal outgrowth measurements. We further undertook transcriptomic analysis of neuroblastoma SH-SY5Y cells, to identify differentially expressed genes in *DDX17*-KD cells compared to controls. Knockdown of *Ddx17* in electroporated mouse neurons *in vivo* showed delayed neuronal migration as well as decreased cortical axon complexity. Mouse primary cortical neurons revealed reduced axon outgrowth upon knockdown of *Ddx17* *in vitro*. The axon outgrowth phenotype was replicated in crispant *ddx17* tadpoles and in heterozygotes. Heterozygous tadpoles had clear neurodevelopmental defects and showed an impaired neurobehavioural phenotype. Transcriptomic analysis identified a statistically significant number of differentially expressed genes involved in neurodevelopmental processes in *DDX17*-KD cells compared to control cells.

We have identified potential neurodevelopment disease-causing variants in a gene not previously associated with genetic disease, *DDX17*. We provide evidence for the role of the gene in neurodevelopment in both mammalian and non-mammalian species and in controlling the expression of key neurodevelopment genes.

Received December 08, 2023. Revised September 05, 2024. Accepted September 15, 2024. Advance access publication October 15, 2024

© The Author(s) 2024. Published by Oxford University Press on behalf of the Guarantors of Brain.

This is an Open Access article distributed under the terms of the Creative Commons Attribution-NonCommercial License (<https://creativecommons.org/licenses/by-nc/4.0/>), which permits non-commercial re-use, distribution, and reproduction in any medium, provided the original work is properly cited. For commercial re-use, please contact reprints@oup.com for reprints and translation rights for reprints. All other permissions can be obtained through our RightsLink service via the Permissions link on the article page on our site—for further information please contact journals.permissions@oup.com.

- 1 Human Genetics and Genomic Medicine, Faculty of Medicine, University of Southampton, Southampton SO16 6YD, UK
- 2 Translational Genomics Group, Broad Institute of MIT and Harvard, Cambridge, MA, 02142, USA
- 3 European Xenopus Resource Centre, School of Environmental and Life Sciences, University of Portsmouth, Portsmouth PO1 2DT, UK
- 4 Physiopathologie et Génétique du Neurone et du Muscle, CNRS UMR5261, INSERM U1315, Institut NeuroMyoGène, Université Claude Bernard Lyon 1, Lyon 69008, France
- 5 Laboratoire de Biologie et Modélisation de la Cellule, Ecole Normale Supérieure de Lyon, CNRS UMR5239, INSERM U1293, Université Claude Bernard Lyon 1, Lyon 69007, France
- 6 INSERM U1052, CNRS UMR5286, Cancer Research Center of Lyon (CRCL), Université Claude Bernard Lyon 1, Lyon 69008, France
- 7 IRCCS Istituto delle Scienze Neurologiche di Bologna, Programma di Neurogenetica, Bologna, 40139, Italy
- 8 Department of Biomedical and Neuromotor Sciences (DIBINEM), University of Bologna, Bologna 40138, Italy
- 9 IRCCS Azienda Ospedaliero-Universitaria di Bologna, Bologna 40138, Italy
- 10 Department of Pediatric Neurosciences, Fondazione IRCCS Istituto Neurologico Carlo Besta, Milan 20133, Italy
- 11 Laboratorio di genetica Medica, Ospedale papà Giovanni XXIII, Bergamo 24127, Italy
- 12 Institute for Clinical Genetics, University Hospital Carl Gustav Carus at the Technische Universität Dresden, Dresden 01307, Germany
- 13 Departments of Pathology and Pediatrics, The Ohio State University, Columbus, OH 43210, USA
- 14 Department of Pediatrics, The Ohio State University, Columbus, OH 43210, USA
- 15 Department of Pediatrics and Clinical Genetics, Nationwide Children's Hospital and Ohio State University, Columbus, OH 43210, USA
- 16 deCODE genetics/Amgen Inc., Reykjavik 102, Iceland
- 17 Division of Neurology, Department of Pediatrics, The Children's Hospital of Philadelphia, Philadelphia, PA 19104, USA
- 18 Department of Neurology, The University of Pennsylvania Perelman School of Medicine, Philadelphia, PA 19104, USA
- 19 Unité Fonctionnelle Innovation en Diagnostic génomique des maladies rares, FHU-TRANSLAD, CHU Dijon Bourgogne, Dijon 21000, France
- 20 INSERM UMR1231 GAD, Université de Bourgogne, Dijon 21000, France
- 21 Medical Genetics Department, University Hospital of Montpellier, Montpellier 34295, France
- 22 Department of Genetic and Molecular Medicine, Landspítali Hospital, Reykjavik, IS-105, Iceland
- 23 Laboratory of Medical Genetics, Translational Cytogenomics Research Unit, Bambino Gesù Children's Hospital, IRCCS, Rome 00146, Italy
- 24 Department of Woman and Child Health and Public Health, Fondazione Policlinico Universitario A. Gemelli IRCCS, Rome 00168, Italy
- 25 Medicine and Surgery School, Università Cattolica del S. Cuore, Rome 00168, Italy
- 26 Rare Diseases Unit, Fondazione Policlinico Universitario A. Gemelli IRCCS, Rome 00168, Italy
- 27 Wessex Clinical Genetics Service, University Hospital Southampton NHS Foundation Trust, Southampton SO16 5YA, UK
- 28 Center for Genomic Medicine, Massachusetts General Hospital, Boston, MA 02114, USA
- 29 Division of Genetics and Genomics, Boston Children's Hospital, Boston, MA, 02115, USA

Correspondence to: Dr Cyril F. Bourgeois

Laboratoire de Biologie et Modélisation de la Cellule, Ecole Normale Supérieure de Lyon, 46 allée d'Italie
Lyon 69007 France

E-mail: cyril.bourgeois@inserm.fr

Keywords: neurodevelopmental/motor delay; RNA helicase; neuronal development; mouse model; xenopus model; novel gene disorder

Introduction

RNA helicases have essential biochemical roles in all aspects of RNA metabolism, including unwinding and annealing RNA molecules and remodelling ribonucleoprotein complexes. The DEAD-box proteins are highly conserved across species, comprising the largest family of RNA helicases.^{1,2} They share 12 conserved motifs, including the signature DEAD (Asp-Glu-Ala-Asp) motif, which altogether form a catalytic site for ATP hydrolysis and an RNA binding site.^{3,4} DDX17, also known as DEAD box protein 17, and its close homologue DDX5, are highly energy-dependent DEAD-box helicases involved in diverse

cellular processes, notably gene expression, biogenesis of miRNAs via their interaction with the Drosha/DGCR8 complex, and the regulation of cell fate switches and biological transitions.⁵⁻⁷ They are coregulators of several transcription factors, including MYOD, a master regulator of muscle differentiation, and SMAD proteins, which mediate transforming growth factor beta induced epithelial-to-mesenchymal transition. Additionally, they are components of the spliceosome and regulate alternative splicing.

DDX17, located on chromosome 22q13.2, has been shown to be involved in the control of repressor element 1-silencing transcription

factor (REST) related processes that are critical during the early phases of neuronal differentiation.⁸ Through its association with REST, DDX17 promotes its binding to the promoter of certain REST-targeted genes and coregulates the transcriptional repression activity of REST. DDX17 and the REST complex are downregulated during neuroblastoma cell differentiation, affecting activation of neuronal genes. Furthermore, DDX17 and DDX5 regulate the expression of multiple proneural microRNAs, which target the REST complex during neurogenesis, implicating DDX17 in neuronal gene repression.⁸ In 2022, Suthapot *et al.*⁹ focused on characterizing chromatin occupancy of DDX17 and DDX5 in human pluripotent stem cells (hPSCs) NTERA2 and their neuronal derivatives. They showed that the expression of both helicases is abundant throughout neural differentiation of the hPSCs NTERA2, preferentially localized within the nucleus and that they occupy chromatin genome-wide at regions associated with genes related to neurogenesis. Both DDX17 and DDX5 are mutually required for controlling transcriptional expression of these neurogenesis-associated genes but are not important for maintenance of the stem cell state of hPSCs. In contrast, they are critical for early neural differentiation of hPSCs, possibly due to their role in the upregulation of key neurogenic transcription factors such as SOX1, SOX21, SOX2, ASCL1, NEUROG2 and PAX6. Critically, DDX17 and DDX5 are important for differentiation of hPSCs toward NESTIN and TUBB3 positive cells, which represent neural progenitors and mature neurons, respectively. However, those studies used a DDX17 and DDX5 co-depletion approach to address the function of these factors in neurogenesis, and information regarding the specific contribution of each helicase to this process is lacking.

Many RNA helicases have been linked to disease (reviewed by Bohnsack *et al.*¹), particularly several neurodevelopmental syndromes involving variants in genes encoding DEAD/DEAH box proteins.^{10–15} However, to date, DDX17 has no disease-gene relationship. The gene is highly constrained for loss-of-function (LoF), i.e. fewer LoF variants in DDX17 are observed in population datasets than would be expected under a null mutation hypothesis [37.7 expected, 1 observed, loss intolerance probability (pLI) = 1.0 in gnomAD]. Genes can be quantified by constraint to LoF using the loss-of-function observed/expected upper-bound fraction (LOEUF) score, which places genes along a continuous spectrum of intolerance to haploinsufficiency.¹⁶ Genes highly constrained for LoF, represented by low LOEUF scores, are highly associated with known haploinsufficient disease genes.^{16,17} However, the majority of genes in the lowest LOEUF decile are not yet associated with a disease phenotype but may be expected to cause disease if mutated through LoF.¹⁸ DDX17 has a LOEUF score of 0.13, suggesting that haploinsufficiency of the gene is not tolerated. Considering its role in neuronal differentiation, muscle differentiation and alternative splicing, one might expect that DDX17 is an essential gene in neurodevelopment and may present such a phenotype in humans. Therefore, we sought to identify and characterize a case-series of patients with LoF variants in DDX17 and perform functional experiments to test the hypothesis that DDX17 represents a new gene-disease relationship in these patients.

Materials and methods

Participant eligibility criteria

Between October 2019 and August 2023, participants were eligible to join our case-series if they had a confirmed *de novo* variant in DDX17, either missense or predicted LoF (canonical splice site, frameshift, stop gained), and the variant was absent from

population databases. With consent, detailed phenotype data were collected on a standardized phenotyping proforma filled in by each participant's referring clinician. In total, 11 eligible patients—who fitted the eligibility criteria—were identified, all of whom consented to participate in our study. Parents and legal guardians of all affected individuals provided written consent for the publication of their results alongside genetic and clinical information. Guardians of Patients 6, 7 and 10 explicitly consented to have photographs published. No follow-up data were collected.

Identifying study participants

We first obtained access to the 100 000 Genomes Project data in October 2019 through membership of a Genomics England Clinical Interpretation Partnership, with approved project RR359: 'Translational genomics: Optimising novel gene discovery for 100 000 rare disease patients'. De-identified whole genome sequencing and phenotype data (stored as human phenotype ontology terms) were accessible in the Genomics England Research Environment. One patient (Patient 3), the index case, was identified with a *de novo* LoF variant in DDX17. Additional study subjects were identified through Matchmaker Exchange after deposition in GeneMatcher between 2019 and 2023.^{19,20}

Sequencing and data analysis

All patients, except for Patient 3, had trio exome sequencing performed. Data processing and variant filtering and prioritization were carried out by in-house pipelines at the respective host centres. Patient 3 had trio whole genome sequencing undertaken as part of the 100 000 Genomes Project²¹ and their data were filtered using the DeNovoLOEUF filtering strategy.¹⁷ DeNovoLOEUF is a tool that can be applied at scale to genomics datasets, extracting rare *de novo* predicted LoF variants in LOEUF-constrained genes.¹⁷

Mouse experiments

Mouse breeding and handling was performed according to experimental protocols approved by the CECCAPP Ethics committee (C2EA15) of the University of Lyon and in accordance with French and European legislation. Detailed methods on *ex vivo* cortical electroporation and primary neuronal cultures, immunostaining, *in utero* cortical electroporation, immunohistochemistry, image acquisition and quantifications and statistical analyses are available in the [Supplementary material](#), 'Methods' section.

Xenopus tropicalis

Adult Nigerian strain *Xenopus tropicalis* were housed within the European *Xenopus* Resource Centre (EXRC; <https://xenopusresource.org>), University of Portsmouth, in recirculating MBKI Ltd systems maintained at 24–25°C (12–12 h light-dark cycle) with 10% daily water changes. All *Xenopus* work was completed in accordance with the Animals (Scientific Procedures) Act 1986 under licence PP4353452 following ethical approval from the University of Portsmouth's Animal Welfare and Ethical Review Body. Detailed methods on the generation of *X. tropicalis* crispant animals and *ddx17* mutant tadpoles, whole-mount *in situ* hybridization, phenotypic analysis, experimental design and statistical analysis are available in the [Supplementary material](#), 'Methods' section.

RNA-seq and RT-qPCR validation

Detailed methods are available in the [Supplementary material, 'Methods' section](#). In summary, human SH-SY5Y neuroblastoma cells were grown and transfected with siRNA against *DDX17*. Depletion of *DDX17* protein was verified by western blot and total RNA was isolated. Directional RNA libraries were prepared from total RNA after removal of ribosomal RNA (lncRNA library, Novogene). High-throughput sequencing of 150 bp paired-end reads was carried out on an Illumina Novaseq 6000 platform (Novogene), generating an average number of 75 million matched pairs of reads per sample. Raw reads were preprocessed, mapped and filtered and then mapped reads were counted for each gene to compute a differential gene expression analysis with the DESeq2²² package ($P < 0.05$, $[\log_2(\text{FC})] \geq 0.50$ and $\text{basemean} \geq 10$). Gene ontology and gene-set enrichment analyses were carried out using the ShinyGO 0.76.3 web interface.²³ Validation of steady-state gene expression was analysed by reverse transcription and qPCR, as described previously.²⁴

Ethics

The index case was identified through the 100 000 Genomes Project [ethics approval by the Health Research Authority (NRES Committee East of England) REC: 14/EE/1112; IRAS: 166 046]. The ethical approval letter is available on request. Additional participants were identified through GeneMatcher. All participants provided written consent for sharing of phenotype and genotype data as approved by their respective institutional review boards. Explicit written consent for sharing of photographs was obtained from individuals providing identifiable information. All *Xenopus* work was completed in accordance with the Home Office Code of Practice under PP4353452 following ethical approval from the University of Portsmouth's Animal Welfare and Ethical Review Body. Mouse breeding and handling was performed according to experimental protocols approved by the CECCAPP Ethics committee (C2EA15) of the University of Lyon, and in accordance with French and European legislation.

Results

We applied the DeNovoLOEUF filtering strategy, as previously described,¹⁷ to 13 494 parent/offspring trios in the 10 000 Genomes Project, focusing on genes with a LOEUF score < 0.2 with no prior disease gene association. We identified one individual harbouring a heterozygous putative LoF (pLoF) variant in *DDX17*. Using the GeneMatcher platform, we identified a further 10 patients all with *de novo* variants in *DDX17* presenting with neurodevelopmental phenotypes. Representatives for these participants were then invited to join our research study and referring clinicians were asked to complete a standardized phenotype table ([Supplementary material](#)). The summary of the phenotypic features of the 11 patients (from 11 independent families) harbouring *de novo* heterozygous variants in *DDX17* are provided in [Table 1](#) and further detailed in the [Supplementary material](#). All variants were absent from gnomAD¹⁶ v2.1.1 and v.3.1.2.

The cohort comprises eight males and three females, all of whom are alive and have a median age of 15 years at the latest available follow-up. The median age of walking was 18 months. Intellectual disability, ranging from moderate-to-mild (IQ 56–83), is prevalent in 7/10 (70%) of patients. Seven of eleven (64%) of the cohort have dysmorphic facial features. Overlapping facial

dysmorphism ([Supplementary material](#)) between patients includes: synophrys, upslanting palpebral fissures, depressed nasal bridge, posteriorly rotated ears, high arched eyebrows, epicanthus, telecanthus, frontal bossing, micrognathia and strabismus. Three patients have fifth finger clinodactyly, two have clubfeet, and three have 2, 3 toe syndactyly (some of these features are shown in [Fig. 1A](#)). Fifty-six per cent (5/9) have attention deficit hyperactivity disorder (ADHD) and 4/11 (36%) have features of autism. Ninety-one per cent (10/11) have delayed speech and language development, 9/11 (82%) have global developmental delay, and 10/11 (91%) have neurodevelopmental delay. Gross motor delay is prevalent in 7/11 (64%) and 9/11 (82%) have fine motor delay. Thirty-six per cent (4/11) have stereotypy and 5/11 (45%) have generalized hypotonia. Patient 9 [height 178 cm ($z = 0.40$); weight, 55.7 kg ($z = -0.89$)] and Patient 4 [height 165 cm (7th percentile); weight, 51.5 kg (4th percentile)] have signs of macrocephaly ([Supplementary material](#)) with z -scores of 3.97 and 3.23, respectively. Patient 5 had signs of macrocephaly at birth, which normalized through infancy. Eight participants had brain MRI scans, of which four patients showed abnormalities including: left lateral compartment greater than right, monolateral temporal cortical dysplasia, asymmetry of the cerebral cortex and right sided non-specific demyelination, generalized brain demyelination, and periventricular white matter hyperintensities ([Supplementary material](#)). No other obvious asymmetry was observed.

Molecular genetic findings

Following variant filtering and prioritization of exome and genome data, no likely pathogenic or pathogenic variants as curated using American College of Medical Genetics and Genomics and the Association for Molecular Pathology (ACMG-AMP) guidelines²⁵ were identified that fully explained the patients' phenotypes. Eleven participating research programmes identified *de novo* variants of uncertain significance in *DDX17* that were of sufficient interest to submit to Matchmaker Exchange. Five variants were pLoF and six variants were missense ([Fig. 1B](#)). Of these missense variants, five are within the helicase domain and evolutionarily conserved from budding yeast to humans ([Supplementary Fig. 1](#)), suggesting that they are important for the structure and/or function of the protein. The sixth missense variant (Patient 11) is located within the carboxyl-terminal part specific to the p82 form of *DDX17*, which has been described in cells from humans and monkeys²⁶ but not annotated in the other species that we considered for the alignment of [Supplementary Fig. 1](#).

Four patients in the cohort had additional variants of uncertain significance reported ([Supplementary material](#)). Patient 7 had compound heterozygous pathogenic variants in *ACADM* associated with medium chain fatty acid dehydrogenase deficiency; NM_000016.5(*ACADM*):c.799G>A,p.(Gly267Arg) and NM_000016.5(*ACADM*):c.985A>G,p.(Lys329Glu). This was detected on newborn screening, was promptly treated, and does not explain their reported phenotype. No other metabolic abnormalities were detected. Patient 3 had a *de novo* Yq11.21-qter deletion and *de novo* Ypter-p11.3 duplication for which the significance is unknown. Patient 6 had an heterozygous variant in *HCFC1* associated with methylmalonic aciduria and homocysteinaemia, and this NM_005334.3(*HCFC1*):c.4418C>T.p.(Thr1407Met) variant has been reported in ClinVar as benign. Patient 10 harboured an heterozygous 16q23.3 (81 477 800–81 552 781) variant of uncertain significance (VUS), inherited from an unaffected mother.

Table 1 Core phenotypic features of cohort with heterozygous de novo variants in DDX17

Patient	Predicted loss-of-function											Missense				
	P1	P2	P3	P4	P5	P6	P7	P8	P9	P10	P11					
Age	3 y 8 m	13 y	13 y 8 m	17 y 6 m	17 y 6 m	4 y	7 y	15 y	16 y	17 y 3 m	23 y					
Sex	F	M	M	M	M	M	M	F	M	F	M					
GRCh38	22:38499457_38499458 del	22:38494928 C>CAT	22:38495939 T>C	22:38494973 TC>T	22:38493717 delT	22:38493736 T>C	22:38495016 C>T	22:38498504 G>A	22:38495900 T>C	22:38498463 T>C	22:38506032 G>T					
Variant c.NM_006386.5	c.481_482 del	c.997_998 dup	c.739-2A>G	c.953 del	c.1380 del	c.1361A>G	c.911G>A	c.608C>T	c.776A>G	c.649A>G	c.206C>A					
Variant p.NP_006377.2	Arg161Gly fs*7	Met333Ile fs*22	splicing	Arg318His fs*36	Asn462Met fs*16	Gln454Arg	Arg304His	Pro203Leu	Gln259Arg	Thr217Ala	Ala69Asp					
Macrocephaly	No	No	No	Yes	At birth	No	No	No	Yes	No	No					
DFF	Yes	Yes	No	Yes	Yes	Yes	No	Yes	No	Yes	No					
Walking	24 m	18 m	16 m	14 m	14 m	>2 y	18 m	2 y	14 m	27 m	nd					
ID	Mild-mod.	No	Mild-mod.	Mild	Mild	nd	No	Moderate	Mild	No	Moderate					
ADHD	No	No	Yes	Yes	Yes	nd	No	No	Yes	nd	Yes					
ASD	No	Yes	Yes	No	No	No	No	No	Yes	Yes	No					
Language	Yes	No	Yes	Yes	Yes	Yes	Yes	Yes	Yes	Yes	Yes					
GDD	Yes	No	No	Yes	Yes	Yes	Yes	Yes	Yes	Yes	Yes					
ND	Yes	Yes	Yes	Yes	Yes	Yes	Yes	Yes	Yes	No	Yes					
GMD	Yes	Yes	No	No	No	Yes	Yes	Yes	Yes	Yes	No					
FMD	Yes	No	Yes	No	Yes	Yes	Yes	Yes	Yes	Yes	Yes					
Stereotypy	No	Yes	No	No	No	Yes	Yes	No	No	Yes	No					
Hypotonia	Yes	Yes	No	No	No	Yes	No	Yes	No	Yes	No					

Age at the last visit, in years (y) and months (m); sex = female (F) or male (M); ADHD = attention deficit hyperactivity disorder; ASD = autism spectrum disorder; DFF = dysmorphic facial features; FMD = fine motor delay; GDD = global developmental delay; GMD = gross motor delay; GRCh38 = genomic coordinates; ID = intellectual disability; Language = delayed speech and language development; ND = neurodevelopmental delay; walking = age walking independently. 'Yes' or 'No' denotes presence or absence of a feature, respectively; nd = not determined. c.NM_006386.5 and p.NP_006377.2 represent MANE transcripts. No protein consequence is available for Patient 3 as it is a splicing variant.

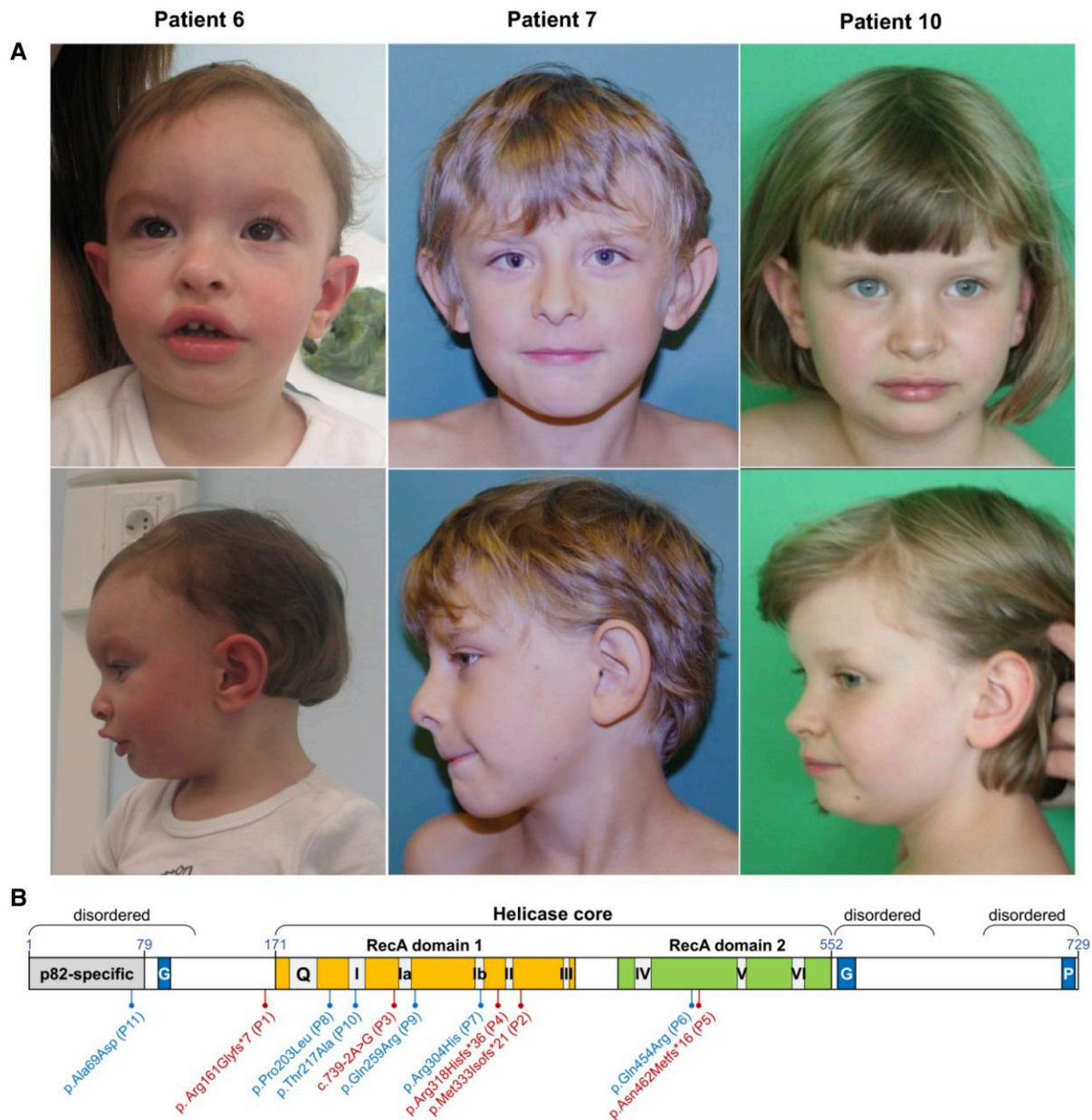


Figure 1 DDX17 patient variants and photographs. (A) Photographs of Patients 6, 7 and 10. Common shared features reported between these patients include posteriorly rotated ears, telecanthus and depressed nasal ridge. Pictures are published with the consent of the families. (B) Gene ideogram, whereby variants in blue are missense and variants in red are loss-of-function.

Ddx17 supports cortical neuron development in the mouse

The identification of several variants in *DDX17* associated with neurodevelopmental features prompted assessment of *DDX17* reduction on cortical development in animal models. We first turned to *in utero* cortical electroporation (IUCE) in the mouse using two distinct shRNA plasmids targeting *Ddx17* (shDDX17 1 or shDDX17 2) (Supplementary Fig. 2). Electroporations were performed at embryonic Day (E)15.5, the developmental stage at which progenitors give rise to callosal-projecting pyramidal neurons. As a control, we used a pLKO.1 vector containing a filler sequence, hence not targeting any mammalian gene. By post-natal Day 21, all electroporated neurons (visualised by mVenus fluorescence) reached the superficial

layers of the cortex (layers II/III), as expected (Fig. 2A). In contrast, we could observe defects in neuronal migration upon knockdown of *Ddx17* (Fig. 2B and C) and after quantification, a statistically significant fraction of neurons did not reach the most superficial cortical layers in conditions electroporated with shRNA plasmids (Fig. 2G). Despite this, neuronal polarization and axon formation was not impaired. In control conditions, axons of layer II/III neurons progress through the corpus callosum to reach the contralateral hemisphere, and branch extensively on ipsilateral layer V (Fig. 2A), as well as contralateral layers II/III (Fig. 2D). In shRNA-electroporated animals, we observed a trend toward a decrease of axon density in the ipsilateral side (Fig. 2B and C, and quantified in Fig. 2H), and especially a strong reduction of contralateral axon density (Fig. 2E and F, and quantified in Fig. 2I). There was no

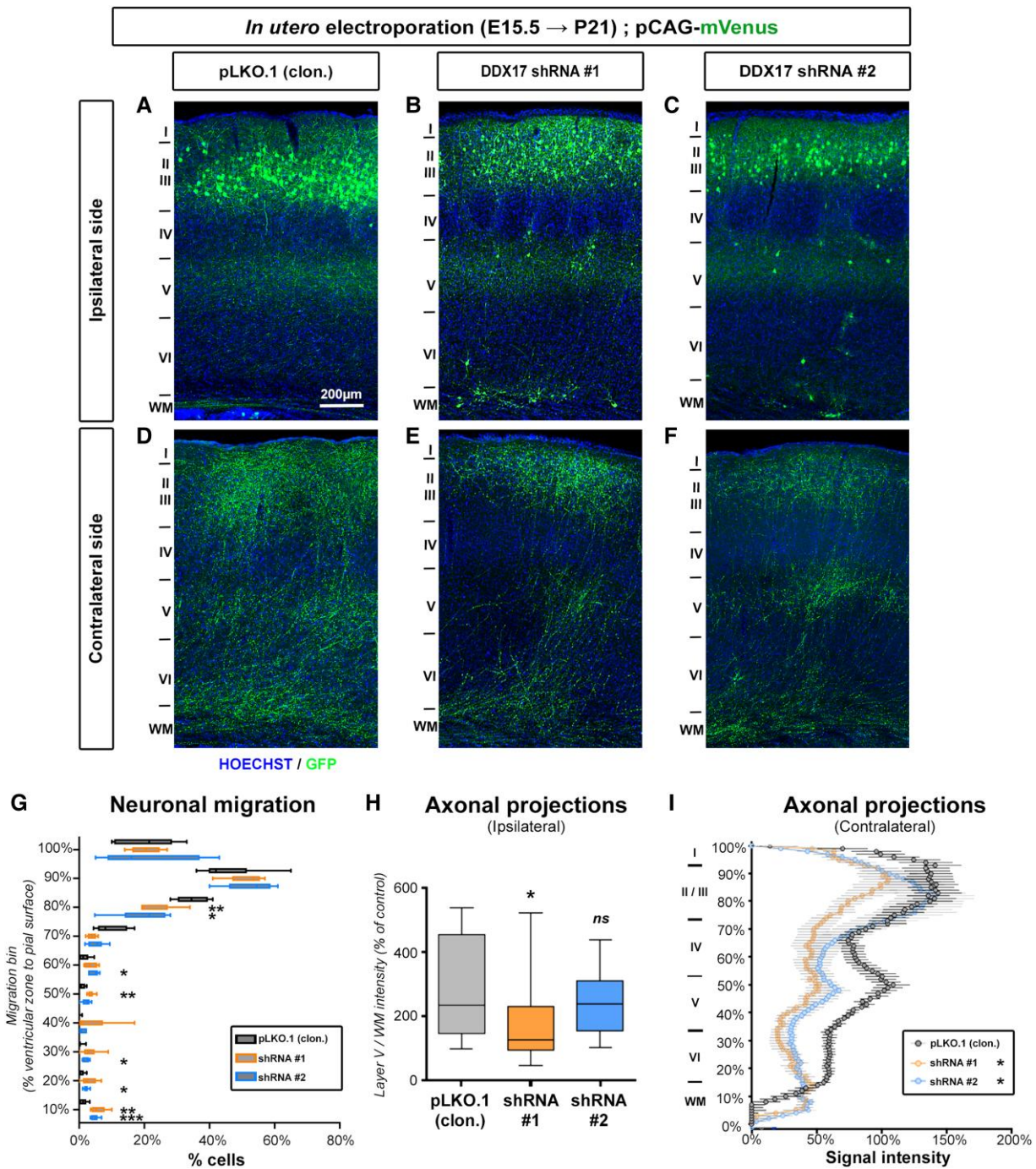


Figure 2 Knockdown of *Ddx17* decreases cortical axon complexity in the mouse *in vivo*. (A–F) Histochemistry of the ipsilateral or contralateral side of mice at post-natal Day 21 (P21) following *in utero* electroporation with pLKO (A and D) or after loss-of-function of *DDX17* (B and C, and E and F) and the fluorescent protein mVenus. (G) Quantification of neuronal migration defects upon knockdown of *Ddx17*. Soma position was quantified on a ventricular zone to pial surface axis. Each bin represents 10% migration. Data: min, max, median, 25th and 75th percentile, $n = 6$ sections out of three animals (two sections per animal). Analysis: two-way ANOVA with multiple comparisons. * $P < 0.05$, ** $P < 0.01$, *** $P < 0.001$. (H) Quantification of normalized mVenus fluorescence in layer V of the ipsilateral cortex (min, max, median, 25th and 75th percentile). $n(\text{pLKO}) = 13$, $n(\text{shDDX17-1}) = 18$, $n(\text{shDDX17-2}) = 25$. Analysis: one-way ANOVA with Dunn’s multiple comparisons. Not significant (ns): $P > 0.05$; * $P < 0.05$. (I) Quantification of normalized mVenus fluorescence along a radial axis in the contralateral cortex (average \pm standard error of the mean) (H) in control condition pLKO or after knockdown of *Ddx17*. $n(\text{pLKO}) = 13$, $n(\text{shDDX17-1}) = 18$, $n(\text{shDDX17-2}) = 25$. Analysis: two-way ANOVA. * $P < 0.05$. E = embryonic Day.

difference in axon density in the white matter (WM), indicating that the same proportion of axons reached the contralateral hemisphere regardless of *Ddx17* expression. Our results demonstrate that *Ddx17* is required for cortical development in the developing mouse brain.

Because the wiring of the brain results from sequential biological processes, defects in the early steps (e.g. neurogenesis or neuronal migration) can lead to alterations in the later biological processes, such as axon development. To make sure that the axonal

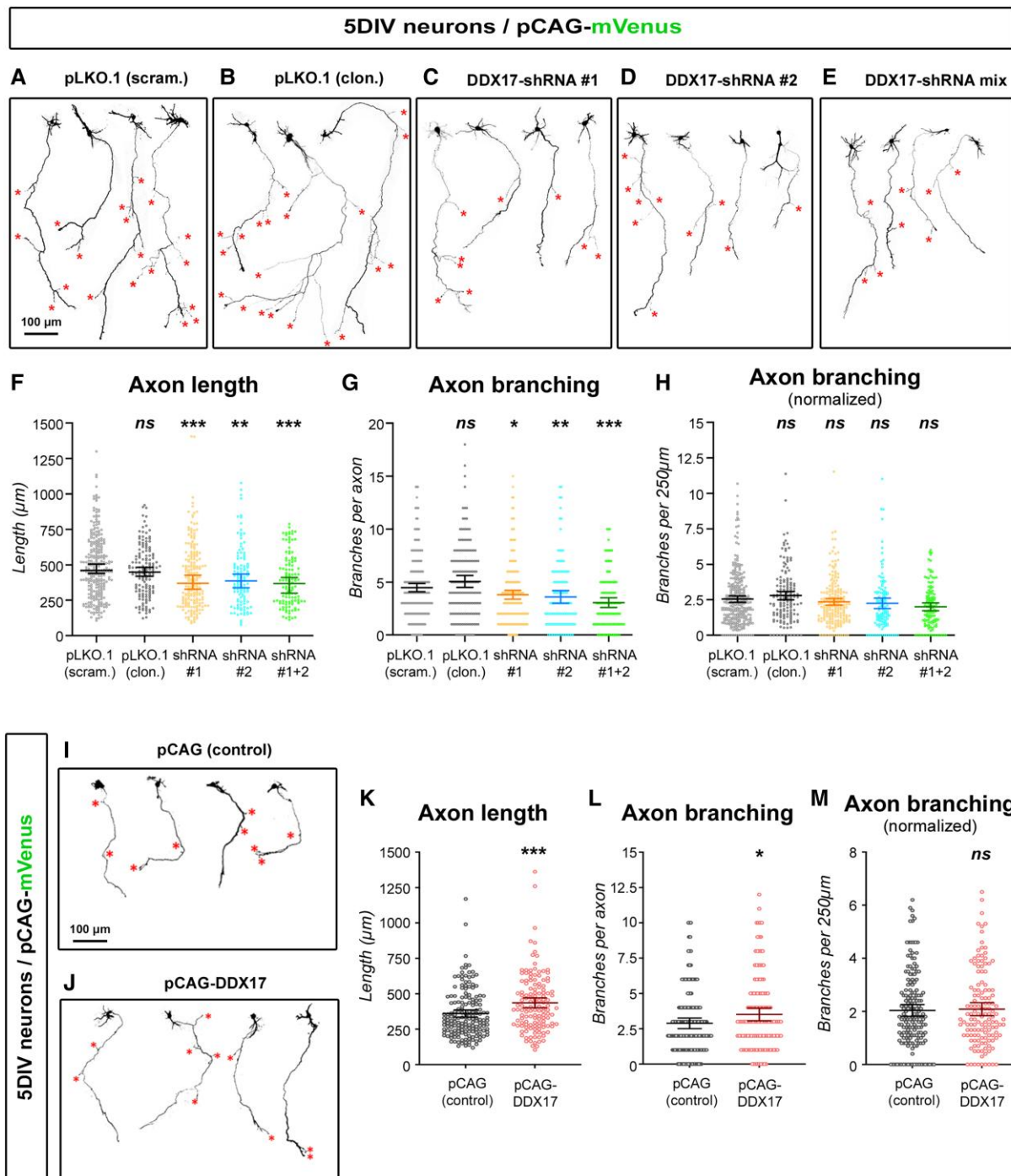


Figure 3 *Ddx17* is necessary and sufficient for axon development. (A–E) Representative images of mVenus expressing cortical neurons [5 days *in vitro* (DIV)] in control condition (pLKO.1 scrambled or pLKO.1 cloning) or after loss-of-function (*Ddx17*-shRNA 1, *Ddx17*-shRNA 2 and *Ddx17*-shRNA 1 + 2 mix). Red asterisks point to collateral branches of the axon. (F–H) Quantification of axon length, number of collateral branches and number of collaterals normalized by axon length of 5DIV neurons in the indicated conditions. Bars represent the average and 95% confidence interval (CI). Statistical tests: Kruskal-Wallis test with Dunn’s post-test (each condition compared to control condition). (I and J) Representative images of mVenus expressing cortical neurons (5DIV) in control conditions, or upon overexpression of *Ddx17*. Red asterisks point to branch/collateral position. (K–M) Quantification of axon length, number of collateral branches and number of collaterals normalized by axon length of 5DIV neurons in the indicated conditions. Bars represent the average and 95% CI. Statistical tests: Kruskal-Wallis test with Dunn’s post-test. (F–H) $n(\text{pLKO.1 scrambling}) = 279$, $n(\text{pLKO.1 cloning}) = 153$, $n(\text{shDDX17 1}) = 193$, $n(\text{shDDX17 2}) = 115$, $n(\text{shDDX17 1 + 2 mix}) = 120$. (K–M) $n(\text{pCAG}) = 168$, $n(\text{pCAG-DDX17}) = 134$. Not significant (ns): $P > 0.05$; ** $P < 0.01$, *** $P < 0.001$.

phenotypes observed *in vivo* do not result from abnormal neuronal migration, we subsequently turned to *in vitro* neuronal cultures, which allow quantitative assessment of axonal development at a single cell resolution. We performed *ex vivo* cortical electroporation

(EVCE) at E15.5 to target neuronal progenitors in the dorsal telencephalon and cultured neurons for 5 days *in vitro* (5DIV). As before, we used the pLKO.1 vector with a filler sequence (pLKO.1 clon.) as a control (Fig. 3A). In addition, and to rule out that activation of the

RISC complex causes non-specific axonal defects, we used another hairpin-forming control vector that does not target a gene in mammalian cells (pLKO.1 scram.) (Fig. 3B). Importantly, DDX17 protein expression was similar in both control conditions (Supplementary Fig. 2). We then quantified the effect of *Ddx17* inhibition on axonal development. While axon morphology was similar with both control conditions (Fig. 3A and B), we observed altered axon development in shRNA-electroporated neurons (Fig. 3C–E). Specifically, the inhibition of DDX17 expression decreased axon length and reduced collateral branch formation (Fig. 3F and G and Supplementary Fig. 3). Two independent shRNA plasmids produced markedly similar phenotypes, indicating that this phenotype is unlikely to be an off-target effect of the shRNAs. Furthermore, we combined shRNA1 and shRNA2 as a way to increase knockdown efficiency and reduce off-target effect, and observed an identical effect on axon length and branching (Fig. 3F and G). When we normalized branch number to axon length, there was still a reduction of collateral branches in shRNA-electroporated neurons compared to the control condition (pLKO.1 scram.), albeit this difference was not statistically significant (Fig. 3H), suggesting that the effect of *Ddx17* inhibition is primarily on axon elongation. Of note, we detected only few neurons positive for the cleaved (activated) form of caspase-3 in control and knockdown conditions, thus ruling out that *Ddx17* inhibition causes neuronal death in our experimental conditions (Supplementary Fig. 3). To confirm this result, we tested the consequence of overexpressing human DDX17 by EVCE. Following electroporation, we observed an increased axon length compared to the control condition, mirroring the effect of *Ddx17* knockdown (Fig. 3I and J, quantified in Fig. 3K). Interestingly, although we counted more branches per neuron (Fig. 3L), axon branching did not differ from the control condition when normalized per axon length (Fig. 3M). Overall, our results demonstrate that *Ddx17* is important for axon development in mouse cortical neurons.

Xenopus ddx17 crispants and heterozygous mutants have reduced axon outgrowth and working memory

To test the effect of LoF *ddx17* variants in a second model, crispant *X. tropicalis* were used. The exon structure of the human and *Xenopus* genes are similar and the proteins produced have 68% amino acid identity with all altered amino acids from patients conserved in the frog with the exception of N462 (Supplementary Fig. 4A). The expression pattern of *ddx17* mRNA has not previously been reported in *Xenopus* and *in situ* hybridization shows it to be expressed most highly in neural tissues, including the migratory neural crest, brain, eye and otic vesicle (see the purple staining in Fig. 4A).

A crispant knockout of *ddx17* was generated using two non-overlapping CRISPR/Cas9 gene-editing complexes designed to disrupt exon 7 (Supplementary Fig. 4B–D) and subsequently these were mated with wild-type frogs to produce F1 mutant heterozygous tadpoles, which more accurately reflect the patient genotype (Supplementary Fig. 5A). The introduction of indels into the *ddx17* locus was tested by Sanger sequencing of the target region and demonstrated strong penetrance of indels in the founder crispant animals (Supplementary Fig. 5B), producing a *ddx17* mosaic crispant knockout model (Xtr.*ddx17*^{em1EXRC}). The heterozygous offspring produced by outcrossing mosaic founders were first identified using the T7E1 mismatch detection assay (Supplementary Fig. 5C), with the genotype confirmed by Sanger sequencing (Supplementary Fig. 5D). This revealed the most frequently

occurring deletions of 5 and 22 bp (Supplementary Fig. 5E), resulting in frameshifts leading to protein truncation within exon 7 (Xtr.*ddx17*^{em2EXRC}). The phenotypes produced by each sgRNA were indistinguishable, showing they were not due to off target effects (Supplementary Fig. 6).

Phenotypically, more than half of the founder (F₀) crispant embryos showed evidence of gastrulation defects (Supplementary Fig. 6A). The remaining animals showed no gross morphological defects (Supplementary Fig. 6B and C). The craniofacial morphology of *ddx17* crispants was tested by injecting CRISPR/Cas9 complexes into one cell of a dividing two-cell embryo. This results in the effects of the protein truncation being concentrated on one side of the embryo along the left-right axis, with the other side acting as an internal control. This makes subtle morphological changes easier to observe, but no altered gross morphology was observed in the crispants (Supplementary Fig. 6C) although there was an altered rate of neuronal outgrowth at early developmental stages (Supplementary Fig. 6D and E). A decrease in head size was observed prior to free-feeding stages [average 5.93 mm² for control tadpoles and 4.89 mm² for crispant tadpoles (NF42, *n* = 16), *t*(30) = 3.85, *P* < 0.001]. This significant decrease in head size was no longer apparent at later stages of development [average 15.9 mm² for control tadpoles and 16.5 mm² for crispant tadpoles (NF48, *n* = 16), *t*(30) = -5.05, *P* = 0.617] (Supplementary Fig. 6F).

F1 mutant *ddx17*^{+/-} tadpoles showed no gross morphological or developmental abnormalities. As there was clear evidence of reduced axon length in electroporated mouse brains deficient in *Ddx17*, neuron outgrowth was also examined in *Xenopus* using an anti-HNK-1 antibody. Embryos injected with control (tyr)²⁷ and *ddx17* gene-editing complexes restricted to one side of the embryo revealed reduced axon outgrowth in *ddx17* crispants on the ipsilateral side (compare the injected and uninjected lateral views in Supplementary Fig. 6D and E). Similarly, in the mutant *ddx17*^{+/-} model, axon outgrowth was visibly and significantly reduced compared with controls at NF24 [controls mean 313; mutants mean 219; *t*(38) = 6.785, *P* < 0.001] and NF26 [controls mean 910; mutants mean 803; *t*(28) = 2.053, *P* = 0.05] (Fig. 4B and C), more embryos are shown in Supplementary Fig. 7A and B. Gross structural differences were not seen in the forebrain, midbrain or hindbrain regions of heterozygous *ddx17*^{+/-} animals, even when bred in a [Xtr.Tg(*tubb2b*:GFP)Amaya] RRID: EXRC_3001 background (Fig. 4D and Supplementary Fig. 7C).

The phenotype of patients with *ddx17* variants include neurodevelopmental deficits and these can now be modelled in *X. tropicalis* using the free-movement pattern (FMP) Y-maze that is already validated.²⁸ Before undertaking this test however, it was necessary to assess whether the tadpoles moved sufficiently. Comparing the movement of control tadpoles and founder F₀ *ddx17* crispant animals at NF48 showed that crispants move less over the 10-min trial period (average 4.0 mm/s for control tadpoles and 2.7 mm/s for crispant tadpoles) [*n* = 48, *t*(82) = -2.6, *P* = 0.012] (Supplementary Fig. 6G). Heterozygous *ddx17*^{+/-} mutant tadpoles behaved differently to the mosaic homozygous animals in some respects; they were observed to move away from tactile stimuli (to the head) and at later stages adopted a normal, head-down filter-feeding posture with the ability to navigate freely within their environment. Further, in the heterozygotes, no abnormalities in locomotive behaviour consistent with descriptors of seizure activity were noted during observation periods.^{29,30} Unlike the founder crispants, the locomotive activity of wild-type and mutant *ddx17*^{+/-} tadpoles was indistinguishable at NF42 when tracked across a 10-min trial period (Fig. 4E).

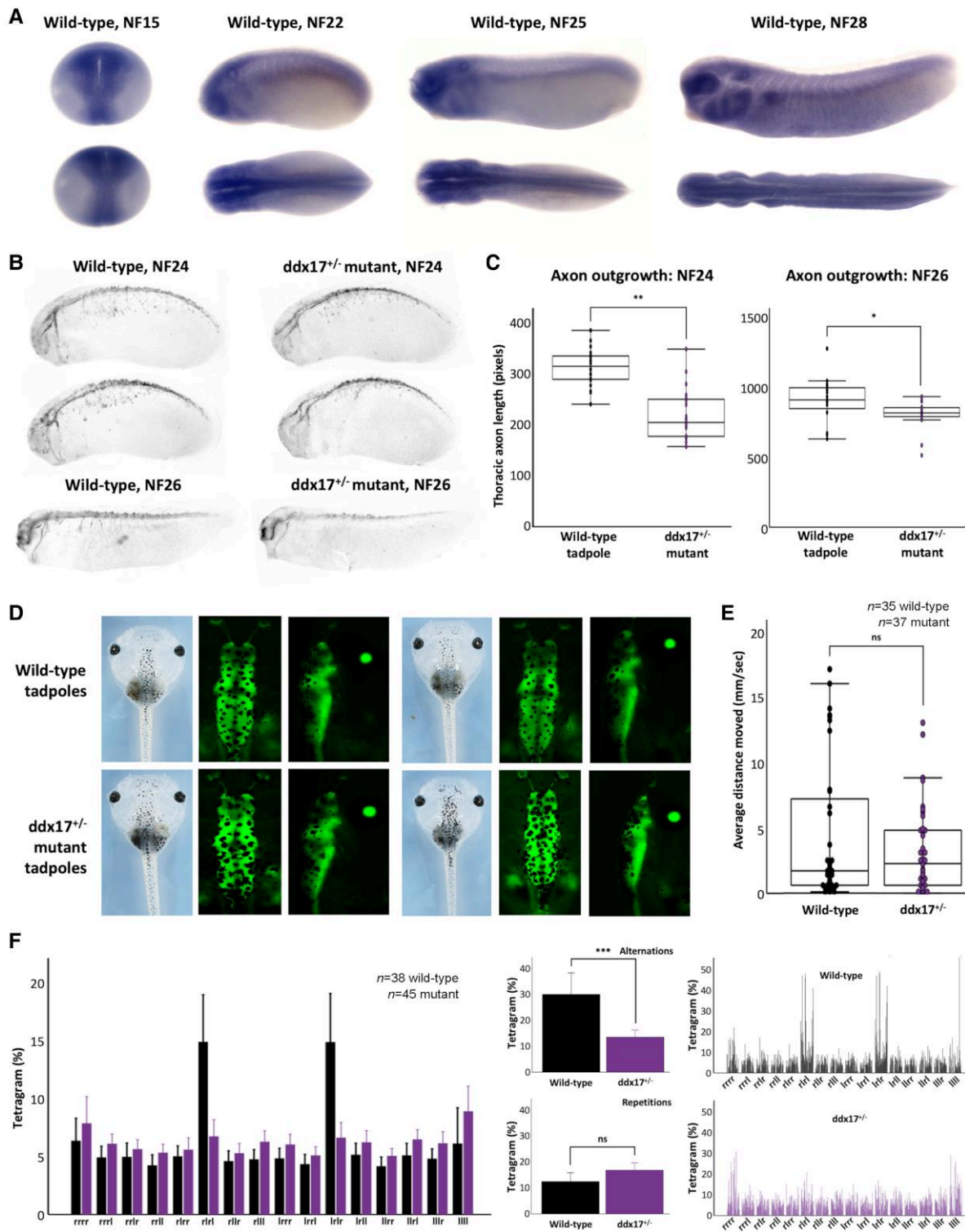


Figure 4 Heterozygous *ddx17*^{-/-} *X. tropicalis* mutants appear morphologically normal but show reduced axon outgrowth and have a working memory deficit. (A) A developmental series of wild-type *X. tropicalis* were fixed and underwent *in situ* hybridization with a probe specific for *ddx17*. The blue stain shows where this gene is expressed. The highest levels of *ddx17* mRNA are in neural tissues, although it is detectable more widely. (B) Control and heterozygous mutant embryos were fixed at the stages shown and stained for neuron bodies and axons using HNK1 monoclonal antibody. The extension of axons ventrally from the neural tube is reduced in mutants at stage NF24 (4/4 embryos) although growth does continue (see stage NF26). (C) For quantification of axon outgrowth, scoring was blind as it was prior to genotyping (see also [Supplementary Fig. 7A and B](#)). (D) Brightfield microscopy showed no clear distinction between control and mutant tadpoles across a range of stages and, when the neural tissue was labelled transgenically, this too failed to reveal any gross morphological distinctions (see [Supplementary Fig. 7C](#)). (E) Tadpoles at stage NF42, similar to those shown in D, underwent automated movement analysis in a Zantiks MWP unit. In all cases, the analysis was performed blind (with genotyping subsequent to measurements) and the black data-points represent wild-type animals with purple showing mutant (*ddx17*^{-/-}) data. (F) The main change caused by heterozygous *ddx17* loss-of-function becomes clear when working memory is tested in the free movement pattern Y-maze; the mutants have lost the alternating search pattern shown by all vertebrates.

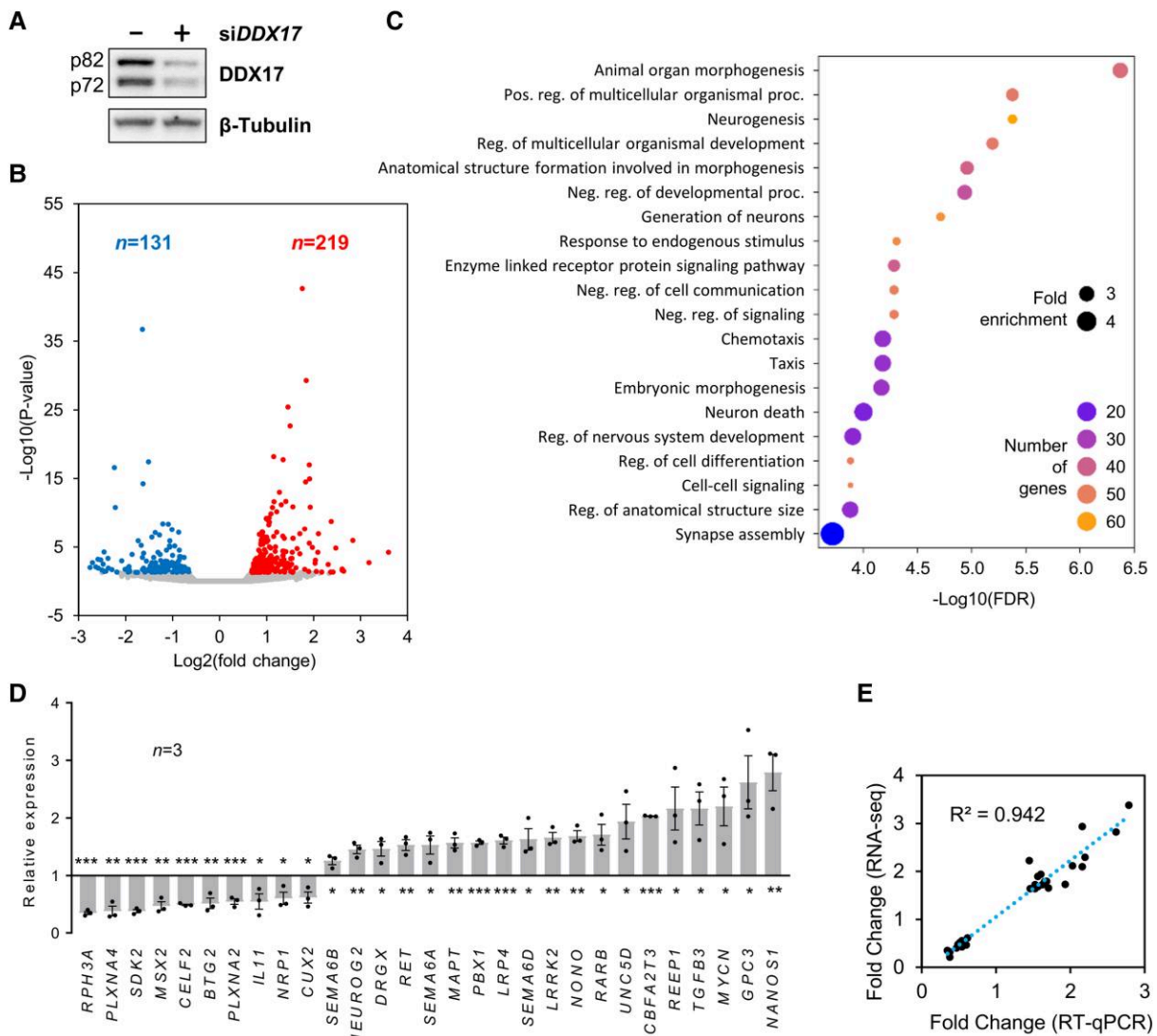


Figure 5 DDX17 controls the expression of genes involved in nervous system development. (A) Western blot showing the siRNA-mediated depletion of DDX17 protein in SH-SY5Y cells. (B) Volcano plot showing the genes that are impacted by DDX17 KD in SH-SY5Y cells, as predicted from the RNA-seq analysis. Significantly altered genes (downregulated in blue and upregulated in red) were identified, as described in the ‘Materials and methods’ section. (C) Gene ontology (GO) analysis using ShinyGO for the genes impacted by DDX17 KD. Only the top 20 of the GO enriched biological processes are shown (see [Supplementary material](#) for the full list of enriched terms). (D) Validation of the effect of DDX17 knockdown on the steady state expression of a selection of genes. RT-qPCR data were first normalized to GAPDH mRNA level in each condition, and the normalized mRNA level of each gene in the DDX17 knockdown condition was then normalized to the control condition, set to 1. Data are expressed as the mean value \pm standard error of the mean of independent experiments ($n=3$). Unpaired Student’s t-test (* $P < 0.05$, ** $P < 0.01$, *** $P < 0.001$). (E) Correlation between the measured fold change of expression (x-axis) and the corresponding predicted fold change value (y-axis) for the 28 genes shown in D.

In a shortened, preliminary FMP Y-maze assay that tests working memory, founder crispant tadpoles performed fewer alternations in their search patterns than controls (average alternations: 22.8% for control tadpoles and 19.5% for crispant tadpoles) [$n=20$, $F(1,33) = 0.366$, $P = 0.550$] and performed more repetitions than the controls (average repetitions 9% for control tadpoles and 12.8% for crispant tadpoles) [$n=0$, $F(1,33) = 3.272$, $P = 0.080$] ([Supplementary Fig. 6H](#)). Neither change was significant in this shortened assay, nonetheless the data suggested a working memory deficit. To test whether this was in fact the case and to circumvent the locomotive deficits in the mosaic crispant tadpoles, the full FMP Y-maze assessment was performed on the mutant *ddx17*^{+/-} tadpoles, which more accurately reflect the human genotype. These demonstrated significantly fewer alternations [$F(1,80) = 14.25$, $P < 0.001$] when compared to

wild-type tadpoles ([Fig. 4F](#)), showing that they have a major deficit in short-term working memory.

Taken together, these data strongly support a causative link between *ddx17* LoF, neurodevelopmental defects and reduced axon growth in *X. tropicalis*.

RNA-seq analysis

Finally, to gain insight into the possible functions and target genes of DDX17 in a human cellular context, we carried out a transcriptomic analysis of neuroblastoma SH-SY5Y cells in which we knocked down the expression of the DDX17 gene, using a mixture of two different siRNAs ([Fig. 5A](#) and [Supplementary Fig. 8](#)). We identified 350 genes that were differentially expressed in DDX17-KD

cells compared to control cells (Fig. 5B and Supplementary material). The functions of this set of genes were significantly associated with developmental processes, in particular the development and functions of the nervous system (Fig. 5C, Supplementary Fig. 9 and Supplementary material). For instance, the expression of several development-associated transcription factors (*MSX2*, *TBX3*, *GATA3*, *FOSL1*, *NEUROG2*, *SMAD6* and *SMAD9*, *SOX13*, *DRGX*, *RARB*, *MYCN*...) was deregulated upon *DDX17* KD. Of note, looking at the molecular functions associated with those genes also revealed the presence of a significant number of trans-membrane receptors (31 genes) and receptor ligands (15 genes) (Supplementary material), including several receptors/ligands associated with axon guidance (*DCC*, *EFNB2*, *PLXNA2* and *PLXNA4*, *SEMA6A* and *SEMA6D*, *RET*, *ROBO2*, *UNC5D*...).

We then analysed separately the subsets of genes of which steady-state expression was negatively (131 genes) or positively (219 genes) altered by *DDX17* KD (Supplementary material). This analysis showed again a significant occurrence of GO terms associated with neurogenesis in both groups of genes, but it also underlined a link between downregulated genes and body morphogenesis, while the group of upregulated genes was associated more specifically to cell-signalling pathways (Supplementary Fig. 10). To validate our computational analysis, we selected 29 genes from the two subgroups of mis-regulated genes and measured their mRNA level by RT-qPCR assays in mock-depleted and *DDX17*-depleted SH-SY5Y cells. Consistently, the expression of each tested gene was altered as predicted from the RNA-seq, with a strong combined correlation score ($R^2 = 0.942$) (Fig. 5D and E).

Collectively, our results show that the *DDX17* gene is involved in several processes during the development of vertebrates, in particular in the development of the nervous system. Our results also strongly suggest this may be due to a role of *DDX17* in regulating the expression of key neurodevelopment-associated genes.

Discussion

To the best of our knowledge, this is the first study to describe *de novo* heterozygous *DDX17* variants associated with features describing a novel neurodevelopmental disorder, adding a new example to the list of helicases associated with such disorders.¹ Using mouse and frog animal models, we provide strong evidence that *DDX17* plays important roles in the developing nervous system. More specifically, *Ddx17* knockdown impaired neuronal migration and axon development in the brain of newborn mice and reduced axon outgrowth and branching in primary cortical neurons *in vitro*. In agreement with these results, crispant tadpole *ddx17* models, including a heterozygous F₁ model, also presented a reduced axon outgrowth phenotype. Heterozygous knockout tadpoles also had clear functional neural defects. Since the region and developmental state of the CNS in the mice and tadpoles in which this effect has been noted are distinct, it suggests that *DDX17* has an important role in widely distributed neurodevelopmental processes. The conservation of function across evolutionarily distant species, such as mice and frogs, strongly support that the role of *DDX17* is conserved in humans too. These *in vivo* results are therefore consistent with the hypothesis that heterozygous LoF *DDX17* variants identified in patients induce a significant alteration of the function of the protein during neuronal development, resulting in the observed phenotype in our cohort.

The phenotype associated with *de novo* variants in *DDX17* is consistent with a neurodevelopmental disorder, typified by

mild-moderate intellectual disability, delayed speech and language development and global developmental delay. Sixty-four per cent (7/11) of the cohort have dysmorphic facial features, although for many this is subtle. Overlapping dysmorphology between patients includes: synophrys, upslanting palpebral fissures, depressed nasal bridge, posteriorly rotated ears, high arched eyebrows, epicanthus, telecanthus and strabismus. Some patients have gross and fine motor delay, generalized hypotonia, stereotypy and evidence of autism spectrum disorder.

There were no substantial differences in phenotype severity between patients harbouring missense variants versus LoF variants, suggesting *DDX17* haploinsufficiency causes the observed phenotype. As all missense variants, but one, are fully conserved from budding yeast to humans and fall within the helicase domain, including two that are within core DEAD box motifs (Fig. 1B and Supplementary Fig. 1), it suggests that they impact the structure and/or activity of this domain in a way that deeply alters the overall function of *DDX17*, similarly to LoF variants. There is evidence that even amino acids not within the core helicase motifs are important for helicase functions, like Pro124 of p72 (Pro203 in p82), which is mutated in Patient 8 and which is involved in ATP binding.³¹ Our preliminary molecular modelling analyses did not reveal any significant modification of the *DDX17* structure in which patient missense mutations were introduced (data not shown). However, our analysis was based on the only known 3D structure of human *DDX17*, which is limited to the helicase core domain.³¹ Recently it has been shown that the two disordered and flexible flanking domains also strongly affect the helicase activity of Dbp2, the yeast *DDX17* orthologue.³² It is thus currently impossible to accurately predict the impact of variants on *DDX17* function, without taking into account the interactions between the structured and unstructured regions of the protein.

We and others have previously shown a role of *DDX17* in the retinoic acid-induced differentiation of neuroblastoma SH-SY5Y and pluripotent embryonal NTERA2 cells, respectively.^{8,9} However, this effect was most evident when *DDX17* knockdown was combined with the concomitant depletion of its paralogue *DDX5*. We now demonstrate that the downregulation of *DDX17* alone is sufficient to alter neuronal development, both *in vivo* and *in vitro*. Both *DDX17* and *DDX5* have largely redundant functions, which probably explains why their joint depletion has such a strong effect compared to single protein depletion. Interestingly, two distinct shRNAs targeting *Ddx17* alter neuronal migration in the mouse cortex. Although shRNA-based strategies are prone to off-target disruption of neuronal migration in the mouse cortex,³³ the migration phenotype is compatible with our previous observation that *DDX17* controls the activity of the REST complex during neurogenesis⁸ and that the REST/CoREST complex regulates neuronal migration.³⁴ Future studies using genetic knockout models will demonstrate the specificity of the migration phenotype. Furthermore, we report that *DDX17* plays a role in axon morphogenesis that is independent of its function in neuronal migration.

Xenopus frogs have been used as pioneer model organisms since the mid-20th century, mainly in discovery research.³⁵ Gene editing was found to be exceptionally effective in them and their application as tools for studying disease has increased.³⁶ *X. tropicalis* are diploid tetrapods with very few gene duplications. Their genome structure has high levels of synteny with humans³⁷ and the initial determination that 80% of human disease genes have orthologues in this species is now thought to be an underestimate.³⁸ We and others have shown them to be highly suited to testing the links

between a variant of uncertain significance and human disease phenotypes.^{28,39} This can often be achieved without breeding the animals due to the efficiency of CRISPR/Cas resulting in very low levels of mosaicism in founders. Hence, they represent a rapid and cost-effective assay for gene-disease associations, filling an important gap between the mouse and zebrafish models. Here we have used mosaic crispant founders and heterozygous F₁ non-mosaic models to test the effect of a truncation in *ddx17* and found a very significant decrease in effective neurodevelopment. If we directly compare mosaic homozygous crispants with non-mosaic F₁ heterozygous animals, there are stronger phenotypic effects in mosaic founder animals. This is a known phenomenon, which may be associated with a failure to activate compensatory mechanisms in mosaic animals, including crispants in another aquatic model, zebrafish (reviewed by Rouf et al.⁴⁰). This suggests that *Xenopus* behave like zebrafish in this respect.

Our data offer some limited insights into the mechanism whereby DDX17 variants affecting its function relate to the disease phenotype. As DDX17 is known to regulate gene expression at multiple levels, the different pathological features associated with DDX17 mutations likely result from the altered expression of some of its target genes and transcripts. Indeed, our transcriptomic analysis showed that 350 genes may be impacted, a large proportion of which are important for development and morphogenesis, and most particularly for neurogenesis. This includes several key transcription factors (*NEUROG2*, *RARB*, *MYCN*...), the deregulation of which could have direct and indirect effects on many other genes in the course of embryonic development. Furthermore, the DDX17-dependent regulation of several genes coding for transmembrane receptors and ligands associated with axon guidance is also of particular significance, considering the altered axonal development observed upon DDX17 knockdown in mice and tadpoles, and the neurological phenotype observed in patients. Whilst further work is needed, the goal of this study is to establish DDX17 as a novel neurodevelopmental disease gene and enable identification of more patients to further elucidate the genotype-phenotype relationship.

Conclusion

We have identified 11 patients with neurodevelopmental phenotypes harbouring monoallelic *de novo* variants in DDX17. Functional experiments (*in vitro* and *in vivo*) show that DDX17 is important in neurodevelopmental processes, in keeping with the observed human phenotype. *Ddx17* knockdown of newborn mice showed impaired axon outgrowth and reduced axon outgrowth and branching was observed in primary cortical neurons *in vitro*. The axon outgrowth phenotype was replicated in crispant *ddx17* tadpoles, including in a heterozygous (F₁) model. Crispant and *ddx17*^{+/-} tadpoles had clear functional neural defects and showed an impaired neurobehavioral phenotype. Transcriptomic analysis further supports the role of DDX17 in neurodevelopmental processes, particularly neurogenesis. These results strongly support that monoallelic LoF variants in DDX17 cause a neurodevelopmental phenotype.

Data availability

Transcriptomic data were deposited in the Gene Expression Omnibus (GEO) database under the record GSE223072. The published article includes all remaining data generated or analysed during this study.

Acknowledgements

Claudia Ciaccio and Stefano D'Arrigo are members of the ITHACA-ERN. Mouse experiments were performed with support from the Service Commun des Animaleries de Rockefeller (SCAR) from the University of Lyon. We acknowledge the CBPSMN (Centre Blaise Pascal de Simulation et de Modélisation Numérique) of the ENS-Lyon for computing resources.

Funding

E.G.S. is supported by The Gerald Kerkut Charitable Trust, The Foulkes Foundation, and a University of Southampton Presidential Scholarship. Mouse work was performed within the framework of the LABEX CORTEX (ANR-11-LABX-0042/ANR-11-IDEX-0007) and with support from the ERC Starting Grant (678302-NEUROMET). M.K. is the recipient of a Marie Skłodowska-Curie Actions grant (101110819). A.O.D.L. and H.L.R. were funded by U01HG011755. A.G. S.E., D.B. and M.G. are funded by the Medical Research Council (MR/V012177/1) and the EXRC is supported by the Wellcome Trust (212942/Z/18/Z) and BBSRC (BB/R014841/1). V.C. was supported by a doctoral fellowship from Fondation pour la Recherche Médicale (FRM). C.F.B. was supported by the french Ligue contre le Cancer (Equipe labellisée).

Competing interests

V.C. acts as consultant and investigator in clinical trials for Chiesi Pharmaceuticals (Leber hereditary optic neuropathy), GenSight Biologics (Leber hereditary optic neuropathy) and Stealth BioTherapeutics (mitochondrial myopathies). H.L.R. received funding for rare disease research from Illumina and Microsoft.

Supplementary material

Supplementary material is available at *Brain* online.

References

- Bohnsack KE, Yi S, Venus S, Jankowsky E, Bohnsack MT. Cellular functions of eukaryotic RNA helicases and their links to human diseases. *Nat Rev Mol Cell Biol.* 2023;24:749–769.
- Bourgeois CF, Mortreux F, Auboeuf D. The multiple functions of RNA helicases as drivers and regulators of gene expression. *Nat Rev Mol Cell Biol.* 2016;17:426–438.
- Hilbert M, Karow AR, Klostermeier D. The mechanism of ATP-dependent RNA unwinding by DEAD box proteins. *Biol Chem.* 2009;390:1237–1250.
- Linder P, Jankowsky E. From unwinding to clamping—The DEAD box RNA helicase family. *Nat Rev Mol Cell Biol.* 2011;12:505–516.
- Fuller-Pace FV. The DEAD box proteins DDX5 (p68) and DDX17 (p72): Multi-tasking transcriptional regulators. *Biochim Biophys Acta.* 2013;1829:756–763.
- Giraud G, Terrone S, Bourgeois CF. Functions of DEAD box RNA helicases DDX5 and DDX17 in chromatin organization and transcriptional regulation. *BMB Rep.* 2018;51:613–622.
- Xing Z, Ma WK, Tran EJ. The DDX5/Dbp2 subfamily of DEAD-box RNA helicases. *Wiley Interdiscip Rev RNA.* 2019;10:e1519.
- Lambert MP, Terrone S, Giraud G, et al. The RNA helicase DDX17 controls the transcriptional activity of REST and the expression of proneural microRNAs in neuronal differentiation. *Nucleic Acids Res.* 2018;46:7686–7700.

9. Suthapot P, Xiao T, Felsenfeld G, Hongeng S, Wongtrakoongate P. The RNA helicases DDX5 and DDX17 facilitate neural differentiation of human pluripotent stem cells NTERA2. *Life Sci*. 2022;291:120298.
10. Karaca E, Harel T, Pehlivan D, et al. Genes that affect brain structure and function identified by rare variant analyses of Mendelian neurologic disease. *Neuron*. 2015;88:499-513.
11. Snijders Blok L, Madsen E, Juusola J, et al. Mutations in DDX3X are a common cause of unexplained intellectual disability with gender-specific effects on wnt signaling. *Am J Hum Genet*. 2015;97:343-352.
12. Lessel D, Schob C, Kury S, et al. De Novo missense mutations in DHX30 impair global translation and cause a neurodevelopmental disorder. *Am J Hum Genet*. 2017;101:716-724.
13. Balak C, Benard M, Schaefer E, et al. Rare De Novo missense variants in RNA helicase DDX6 cause intellectual disability and dysmorphic features and lead to P-body defects and RNA dysregulation. *Am J Hum Genet*. 2019;105:509-525.
14. Paine I, Posey JE, Grochowski CM, et al. Paralog studies augment gene discovery: DDX and DHX genes. *Am J Hum Genet*. 2019;105:302-316.
15. Burns W, Bird LM, Heron D, et al. Syndromic neurodevelopmental disorder associated with de novo variants in DDX23. *Am J Med Genet A*. 2021;185:2863-2872.
16. Karczewski KJ, Francioli LC, Tiao G, et al. The mutational constraint spectrum quantified from variation in 141,456 humans. *Nature*. 2020;581:434-443.
17. Seaby EG, Thomas NS, Webb A, et al. Targeting de novo loss-of-function variants in constrained disease genes improves diagnostic rates in the 100 000 Genomes Project. *Hum Genet*. 2023;142:351-362.
18. Seaby EG, Smedley D, Taylor Tavares AL, et al. A gene-to-patient approach uplifts novel disease gene discovery and identifies 18 putative novel disease genes. *Genet Med*. 2022;24:1697-1707.
19. Philippakis AA, Azzariti DR, Beltran S, et al. The matchmaker exchange: A platform for rare disease gene discovery. *Hum Mutat*. 2015;36:915-921.
20. Sobreira N, Schiettecatte F, Valle D, Hamosh A. GeneMatcher: A matching tool for connecting investigators with an interest in the same gene. *Hum Mutat*. 2015;36:928-930.
21. Investigators GPP, Smedley D, Smith KR, et al. 100 000 genomes pilot on rare-disease diagnosis in health care—Preliminary report. *N Engl J Med*. 2021;385:1868-1880.
22. Love MI, Huber W, Anders S. Moderated estimation of fold change and dispersion for RNA-seq data with DESeq2. *Genome Biol*. 2014;15:550.
23. Ge SX, Jung D, Yao R. ShinyGO: A graphical gene-set enrichment tool for animals and plants. *Bioinformatics*. 2020;36:2628-2629.
24. Terrone S, Valat J, Fontrodona N, et al. RNA helicase-dependent gene looping impacts messenger RNA processing. *Nucleic Acids Res*. 2022;50:9226-9246.
25. Richards S, Aziz N, Bale S, et al. Standards and guidelines for the interpretation of sequence variants: A joint consensus recommendation of the American College of Medical Genetics and Genomics and the Association for Molecular Pathology. *Genet Med*. 2015;17:405-424.
26. Uhlmann-Schiffler H, Rossler OG, Stahl H. The mRNA of DEAD box protein p72 is alternatively translated into an 82-kDa RNA helicase. *J Biol Chem*. 2002;277:1066-1075.
27. Nakayama T, Blitz IL, Fish MB, et al. Cas9-based genome editing in *Xenopus tropicalis*. *Methods Enzymol*. 2014;546:355-375.
28. Ismail V, Zachariassen LG, Godwin A, et al. Identification and functional evaluation of GRIA1 missense and truncation variants in individuals with ID: An emerging neurodevelopmental syndrome. *Am J Hum Genet*. 2022;109:1217-1241.
29. Hewapathirane DS, Haas K. The albino *Xenopus laevis* tadpole as a novel model of developmental seizures. In: Se B, ed. *Animal models of epilepsy*. Humana Press; 2009:45-57.
30. Panthi S, Chapman PA, Szyszka P, Beck CW. Characterisation and automated quantification of induced seizure-related behaviours in *Xenopus laevis* tadpoles. *J Neurochem*. 2024;168:4014-4024.
31. Ngo TD, Partin AC, Nam Y. RNA specificity and autoregulation of DDX17, a modulator of MicroRNA biogenesis. *Cell Rep*. 2019;29:4024-4035.e4025.
32. Song QX, Liu NN, Liu ZX, et al. Nonstructural N- and C-tails of Dbp2 confer the protein full helicase activities. *J Biol Chem*. 2023;299:104592.
33. Baek ST, Kerjan G, Bielas SL, et al. Off-target effect of doublecortin family shRNA on neuronal migration associated with endogenous microRNA dysregulation. *Neuron*. 2014;82:1255-1262.
34. Volvert ML, Prevot PP, Close P, et al. MicroRNA targeting of CoREST controls polarization of migrating cortical neurons. *Cell Rep*. 2014;7:1168-1183.
35. De Robertis EM, Gurdon JB. A brief history of *Xenopus* in biology. *Cold Spring Harb Protoc*. 2021;2021:469-472.
36. Kostiuik V, Khokha MK. *Xenopus* as a platform for discovery of genes relevant to human disease. *Curr Top Dev Biol*. 2021;145:277-312.
37. Hellsten U, Harland RM, Gilchrist MJ, et al. The genome of the western clawed frog *Xenopus tropicalis*. *Science*. 2010;328:633-636.
38. Blum M, Ott T. *Xenopus*: An undervalued model organism to study and model human genetic disease. *Cells Tissues Organs*. 2018;205:303-313.
39. Macken WL, Godwin A, Whewey G, et al. Biallelic variants in COPB1 cause a novel, severe intellectual disability syndrome with cataracts and variable microcephaly. *Genome Med*. 2021;13:34.
40. Rouf MA, Wen L, Mahendra Y, et al. The recent advances and future perspectives of genetic compensation studies in the zebrafish model. *Genes Dis*. 2023;10:468-479.